

Simple quantum error detection and correction for superconducting qubits

Kyle Keane and Alexander N. Korotkov

*Department of Electrical Engineering and Department of Physics & Astronomy,
University of California, Riverside, California 92521*

(Dated: July 14, 2018)

We analyze simple quantum error detection and quantum error correction protocols relevant to current experiments with superconducting qubits. We show that for qubits with energy relaxation the repetitive N -qubit codes cannot be used for quantum error correction, but can be used for quantum error detection. In the latter case it is sufficient to use only two qubits for the encoding. In the analysis we demonstrate a useful technique of unraveling the qubit energy relaxation into “relaxation” and “no relaxation” scenarios. Also, we propose and numerically analyze several two-qubit algorithms for quantum error detection/correction, which can be readily realized at the present-day level of the phase qubit technology.

PACS numbers: 03.67.Pp, 03.67.Lx, 85.25.Cp

I. INTRODUCTION

Quantum error correction [1] (QEC) is an unavoidable procedure in a practical quantum computer [2, 3]. The standard QEC [1, 2] includes encoding a logical qubit in several physical qubits, measuring the error syndrome using ancillary qubits, and then applying a correction operation, which depends on the measurement result. (A promising variation of this idea are the so-called surface codes [4].) Unfortunately, QEC is very difficult experimentally [5–15], and some simplifications are often used. Let us mention three of them, all of which have been introduced in Ref. [5]. First, instead of using additional qubits for the error syndrome, in a “compact” scheme the same physical qubits can be used for the encoding and error syndrome measurement; this is done by decoding the encoded state after a possible error occurs. Second, since a single-shot measurement of a qubit state is often difficult, the standard QEC can be replaced by measurement-free QEC, in which the measurement and correction are substituted by a quantum controlled operation (e.g. the Toffoli gate). Third, a favorable type of error (against which the code protects) is often simulated by applying a certain unitary rotation, with the rotation angle corresponding to the error strength.

Measurement-free QEC experiments in nuclear magnetic resonance (NMR) systems [5–8] have been performed for over a decade, but only with ensembles of quantum systems [16]. Using trapped ions, a three-qubit QEC experiment with actual measurement was realized [9], and recently a measurement-free QEC procedure with several error correction cycles was demonstrated [10]. In linear optics systems, the QEC experiments include two-qubit protection against “accidental” measurement [11], continuous-variable adaptation of the 9-qubit Shor’s code [12], continuous-variable erasure-correcting code [13], and eight-photon topological error correction [14]. A three-qubit measurement-free QEC protocol has been recently demonstrated with superconducting “transmon” qubits [15].

With the rapid progress in experiments with supercon-

ducting qubits [17, 18], QEC with actual measurements is becoming feasible in these systems in the reasonably near future. The subject of this paper is the analysis of several simple quantum error correction/detection protocols relevant to future experiments with superconducting qubits, mainly superconducting phase qubits [19]. (Some results of this paper have been reported earlier [20].)

In the past, pure dephasing was by far the dominant source of decoherence in superconducting qubits, and QEC protecting against pure dephasing would be most important. An example of such a procedure was considered theoretically in Ref. [21]. The idea was to use the standard 3-qubit repetitive code, which protects from bit flips (i.e. X -rotations). By using additional Hadamard gates for each physical qubit, the X -rotations are converted into Z -rotations, and therefore the same code can be used to protect against pure dephasing.

In recent years, pure dephasing in superconducting qubits was significantly reduced by various technological advances [17, 18], and now energy relaxation is becoming most important. In particular, when quantum information is stored in a superconducting resonator [22, 23], pure dephasing is negligible in comparison with energy relaxation. This is why in the first part of this paper (Sec. II) we focus on the operation of repetitive N -qubit quantum codes in the presence of energy relaxation. Repetitive codes are chosen because of their relative simplicity in the encoding and decoding (unfortunately, the standard 5-qubit or 7-qubit stabilizer codes [1, 2, 24] are not feasible for superconducting qubits in the near future). To reduce the number of qubits in a procedure we use the standard compact scheme [5, 21], in which the ancilla qubits used for encoding are also used for the error syndrome measurement. We assume that the energy relaxation happens at zero temperature, which is essentially the case for superconducting phase qubits, since the typical qubit frequency is ~ 6 GHz, and therefore the energy $\hbar\omega \simeq 0.3$ K is much larger than the experimental temperature of ~ 50 mK.

Even though energy relaxation may look similar to a bit-flip, it actually can be thought of as a combination

of two quantum errors: bit-flip and bit-phase-flip (which correspond to X -rotation and Y -rotation). This is the reason why, as we show later explicitly, repetitive codes do not work for QEC against energy relaxation. However, these codes can be efficiently used for quantum error detection (QED). In QED we detect that an error happened but cannot restore the undamaged quantum state (in particular, the QED idea was implemented in Ref. [25] for phase errors in liquid-state NMR and has been recently investigated in Ref. [13] for detecting photon erasures). Even though QED is of much more limited use than QEC, it is still an interesting procedure, and experimentally can be considered as a first step towards full QEC. We show that for QED against energy relaxation it is sufficient to use 2-qubit encoding and that there is not much benefit to use more qubits, unless a somewhat more sophisticated procedure is used.

Our analysis in Sec. II is based on unraveling the qubit energy relaxation into the “relaxation” and “no relaxation” scenarios. This unraveling is quite different (and more difficult) than, for example, unraveling of pure dephasing into the “phase flip” and “no phase flip” scenarios. The main reason for the difference is that the unraveled states for the energy relaxation are related to the initial state in a non-unitary way.

In Sec. III we focus on simple two-qubit QEC/QED protocols, somewhat similar to those in Ref. [25], which can be readily implemented using the present-day technology of phase qubits [23]. Realistic experimental parameters are used in the numerical simulation of these protocols. In the first protocol and its variations, we assume that as in most of the previous experiments [5–15] the errors are intentionally induced by particular operations pretended to be unknown. The algorithms can mainly be used for QED; however, when the type of particular error is known (which is the case for intentional errors in an experiment), the algorithms can also be used for QEC. We also analyze numerically the operation of a protocol, in which the errors during a storage period are due to actual energy relaxation of two qubits (assuming storage in resonators of a ReZQu-architecture device [23, 26] with phase qubits). This protocol can only be used in the QED mode. The main result of the simulations is that the analyzed protocols can be realized at the present-day level of phase qubit technology. Section IV is a conclusion. Some mathematical details of the analysis are discussed in the Appendix.

II. REPETITIVE CODING FOR ENERGY RELAXATION

In this section we analyze the operation of repetitive N -qubit encoding in the presence of (Markovian) zero-temperature energy relaxation. The procedure is shown in Fig. 1. The goal is to preserve an arbitrary initial state

$$|\psi_{\text{in}}\rangle = \alpha|0\rangle + \beta|1\rangle \quad (1)$$

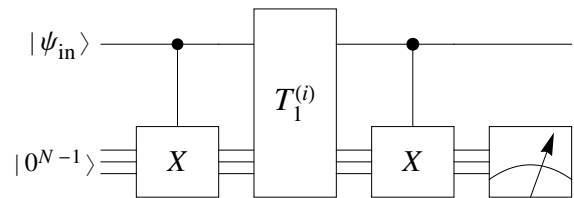


FIG. 1: N -qubit repetitive coding algorithm with one control qubit initially containing the quantum information. The controlled- X block represents CNOT gates from the main qubit to each ancilla qubit individually. $T_1^{(i)}$ represents energy relaxation of the i th qubit ($i = 1$ for the main qubit, $i \geq 2$ for ancilla qubits).

of the main (upper) qubit, where $|0\rangle$ is the ground state and $|1\rangle$ is the excited state. In this paper we consider only preservation of the initial state (“memory” operation), so in discussing the fidelity of a procedure we always imply comparison with the ideal memory operation.

The encoding in Fig. 1 is performed with $N - 1$ controlled-NOT (CNOT) gates, acting on $N - 1$ ancilla qubits, which all start in the state $|0\rangle$. This produces the N -qubit wavefunction $\alpha|0^N\rangle + \beta|1^N\rangle$, where the notation $|x^N\rangle$ represents the product-state of N qubits, all being in the state x . After the encoding, all qubits are subjected to decoherence due to zero-temperature energy relaxation with relaxation time $T_1^{(i)}$ for the i th qubit, $i = 1, 2, \dots, N$. We will mostly consider the case when the decoherence is the same for all qubits, $T_1^{(i)} = T_1$. After the decoherence during time t , the logic state is decoded by using $N - 1$ CNOT gates in the same way as was done for the encoding, and all $N - 1$ ancilla qubits are measured in the computational basis. In the absence of decoherence ($t = 0$) the state after decoding is $(\alpha|0\rangle + \beta|1\rangle)|0^{N-1}\rangle$, so that the initial state of the main qubit is restored and the measurement results for all ancillas are 0. The decoherence disturbs the final state, which probabilistically changes the measurement results and the corresponding final states of the main qubit.

Even when the measurement result is all $N - 1$ zeros (for which we will use the bold-font notation $\mathbf{0}$), the state of the main qubit is not exactly $|\psi_{\text{in}}\rangle$; however, we will see that it is close to $|\psi_{\text{in}}\rangle$. A measurement result different from $\mathbf{0}$ indicates an error. There are three ways to handle this situation. First, the measurement result can be simply ignored; in this case there is obviously no benefit from using the encoding/decoding procedure. Second, we can reject such cases and keep only realizations with the measurement result $\mathbf{0}$; we will refer to this selective procedure as quantum error detection. Third, we can apply a quantum operation to the main qubit to make its state closer to $|\psi_{\text{in}}\rangle$. This operation will depend on the measurement result, and the procedure is then quantum error correction.

For simplicity in this section we neglect decoher-

ence (and other imperfections) during encoding, decoding, and measurement; it will be taken into account in the next section when we will discuss realistic experiments with phase qubits. To characterize the efficiency of a procedure either the quantum process tomography (QPT) fidelity F_χ or the average state fidelity F_{av} can be used. The QPT fidelity is usually defined as [2, 27] $F_\chi = \text{Tr}(\chi^{\text{desired}}\chi)$, where χ is the process matrix and χ^{desired} in our case corresponds to the ideal quantum memory operation, i.e. no evolution of the logic qubit. The average state fidelity is [2, 27] $F_{\text{av}} = \int \text{Tr}(\rho_{\text{fin}}U_0|\psi_{\text{in}}\rangle\langle\psi_{\text{in}}|U_0^\dagger) d|\psi_{\text{in}}\rangle$, where $U_0 = \mathbb{1}$ is the desired unitary operator, $\rho_{\text{fin}}(|\psi_{\text{in}}\rangle\langle\psi_{\text{in}}|)$ is the actual mapping from the initial state to the final density matrix ρ_{fin} , and the normalized integral is over all pure initial states $|\psi_{\text{in}}\rangle$ using the Haar measure. For a trace-preserving operation $F_{\text{av}} = (F_\chi d + 1)/(d + 1)$, where $d = 2$ is the dimension of our Hilbert space [27]. This relation holds for QEC and/or when the measurement result is ignored. However, for the QED procedure there is a problem [29] in defining the QPT fidelity F_χ because the procedure is selective; then the quantum operation for normalized states is not linear and the corresponding (trace-preserving) matrix χ cannot be defined rigorously. In this case we *define* F_χ via the average state fidelity,

$$F_\chi = (3F_{\text{av}} - 1)/2, \quad (2)$$

as for a trace-preserving operation.

A. Single-qubit relaxation

Before calculating the fidelity of the QEC and QED procedures, let us calculate the quantum memory fidelity of a single qubit, without any encoding. We also consider first this simple case to demonstrate a technique of unraveling the evolution due to energy relaxation, which is later used for N -qubit encoding.

After time t an initial state $|\psi_{\text{in}}\rangle = \alpha|0\rangle + \beta|1\rangle$ becomes a density matrix (here the upper row and left column correspond to the excited state $|1\rangle$)

$$\rho_{\text{fin}} = \begin{pmatrix} |\beta|^2 e^{-t/T_1} & \alpha^* \beta e^{-t/2T_1} \\ \alpha \beta^* e^{-t/2T_1} & |\alpha|^2 + |\beta|^2 (1 - e^{-t/T_1}) \end{pmatrix}, \quad (3)$$

which can be represented using the Kraus operators:

$$\rho_{\text{fin}} = A_r \rho_{\text{in}} A_r^\dagger + A_n \rho_{\text{in}} A_n^\dagger, \quad (4)$$

$$A_r = \begin{pmatrix} 0 & 0 \\ \sqrt{p} & 0 \end{pmatrix}, \quad A_n = \begin{pmatrix} \sqrt{1-p} & 0 \\ 0 & 1 \end{pmatrix}, \quad (5)$$

where $p = 1 - e^{-t/T_1}$, $\rho_{\text{in}} = |\psi_{\text{in}}\rangle\langle\psi_{\text{in}}|$, and the Kraus operators satisfy the completeness relation $A_r^\dagger A_r + A_n^\dagger A_n = \mathbb{1}$. This representation has an obvious interpretation as two scenarios of the evolution. The first term in Eq. (4) corresponds to qubit relaxation into the ground state $|0\rangle$ with probability $P_r = |\beta|^2 p$. The second term is the no-relaxation scenario, which occurs with the remaining

probability $P_n = |\alpha|^2 + |\beta|^2 (1-p) = 1 - P_r$ and transforms the qubit into the state

$$|\psi_n\rangle = \frac{A_n |\psi_{\text{in}}\rangle}{\sqrt{P_n}} = \frac{\alpha|0\rangle + \beta\sqrt{1-p}|1\rangle}{\sqrt{P_n}}. \quad (6)$$

The non-unitary evolution $|\psi_{\text{in}}\rangle \rightarrow |\psi_n\rangle$ is essentially the same as for a partial collapse due to a null-result measurement in the experiment of Ref. [30].

Now let us find the averaged state fidelity $F_{\text{av}} = \text{Tr}(\rho_f |\psi_{\text{in}}\rangle\langle\psi_{\text{in}}|)$ using unraveling into the relaxation and no-relaxation scenarios. With probability P_r the state fidelity is $F_{\text{st},r} = |\langle 0|\psi_{\text{in}}\rangle|^2 = |\alpha|^2$, and with probability P_n the state fidelity is $F_{\text{st},n} = |\langle\psi_n|\psi_{\text{in}}\rangle|^2 = (|\alpha|^2 + \sqrt{1-p}|\beta|^2)^2/P_n$. Therefore for an initial state $|\psi_{\text{in}}\rangle$ the state fidelity is

$$F_{\text{st}} = F_{\text{st},r} P_r + F_{\text{st},n} P_n \quad (7)$$

$$= |\alpha|^2 |\beta|^2 p + |\alpha|^4 + (1-p)|\beta|^4 + 2|\alpha|^2 |\beta|^2 \sqrt{1-p}, \quad (8)$$

and the average fidelity $F_{\text{av}} = \overline{F_{\text{st}}}$ can be calculated by averaging $|\alpha|^4$, $|\beta|^4$, and $|\alpha|^2 |\beta|^2$ over the Bloch sphere. These averages (including some others for completeness and later use) are

$$\overline{|\alpha|^4} = \overline{|\beta|^4} = \int_0^\pi \frac{(1 + \cos \theta)^2}{4} \frac{\sin \theta}{2} d\theta = \frac{1}{3}, \quad (9)$$

$$\overline{|\alpha|^2 |\beta|^2} = \int_0^\pi \frac{(1 + \cos \theta)(1 - \cos \theta)}{4} \frac{\sin \theta}{2} d\theta = \frac{1}{6}, \quad (10)$$

$$\overline{|\alpha|^2} = \overline{|\beta|^2} = \frac{1}{2}, \quad \overline{|\alpha|^6} = \overline{|\beta|^6} = \frac{1}{4}, \quad (11)$$

$$\overline{|\alpha|^2 |\beta|^4} = \overline{|\alpha|^4 |\beta|^2} = \frac{1}{12}, \quad \overline{|\alpha|^4 |\beta|^4} = \frac{1}{30}, \quad (12)$$

$$\overline{1/(A + B|\beta|^2)} = (1/B) \ln(1 + B/A), \quad (13)$$

$$\overline{|\beta|^2/(A + B|\beta|^2)} = (1/B) - (A/B^2) \ln(1 + B/A), \quad (14)$$

$$\overline{|\beta|^4/(A + B|\beta|^2)} = \frac{1}{2B} - \frac{A}{B^2} + \frac{A^2}{B^3} \ln(1 + B/A), \quad (15)$$

$$\overline{\frac{|\alpha|^4}{A + B|\beta|^2}} = \frac{-3}{2B} - \frac{A}{B^2} + \frac{(A+B)^2}{B^3} \ln(1 + B/A), \quad (16)$$

$$\overline{\frac{|\alpha|^2 |\beta|^2}{A + B|\beta|^2}} = \frac{1}{2B} + \frac{A}{B^2} - \frac{A(A+B)}{B^3} \ln(1 + B/A), \quad (17)$$

where A and B are constants, and we used integration over the Bloch-sphere polar angle θ , so that $|\alpha|^2 = (1 + \cos \theta)/2$ and $|\beta|^2 = (1 - \cos \theta)/2$.

Applying the averages (9) and (10) to Eq. (8), we obtain the average state fidelity

$$F_{\text{av}} = \frac{2}{3} + \frac{\sqrt{1-p}}{3} - \frac{p}{6}. \quad (18)$$

Actually, there is an easier way to obtain this result. Instead of averaging F_{st} over the Bloch sphere, it is sufficient [27, 28] (see also Appendix) to calculate the average only over 6 initial states: $|0\rangle$, $|1\rangle$, $(|0\rangle \pm |1\rangle)/\sqrt{2}$, and $(|0\rangle \pm i|1\rangle)/\sqrt{2}$. However, in our further analysis this trick

does not always help, so we prefer the full integration over the Bloch sphere. Using Eq. (2) it is easy to convert Eq. (18) into the QPT fidelity: $F_\chi = (1 + \sqrt{1-p} - p/2)/2$. Note that for small p

$$F_{\text{av}} \approx 1 - \frac{p}{3}, \quad F_\chi \approx 1 - \frac{p}{2}, \quad p \approx \frac{t}{T_1} \ll 1. \quad (19)$$

The average state fidelity (18) is averaged over the two scenarios. Let us now discuss the average state fidelity in each scenario separately, having in mind a gedanken experiment in which an emitted photon or phonon is always captured and recorded, thus allowing us to distinguish the two scenarios. If the relaxation has happened, then $F_{\text{st,r}} = |\alpha|^2$ and averaging this over the Bloch sphere we obtain

$$F_{\text{av,r}} = \overline{|\alpha|^2} = 1/2. \quad (20)$$

Similarly, for the no-relaxation scenario $F_{\text{av,n}} = \overline{(|\alpha|^2 + \sqrt{1-p}|\beta|^2)^2 / [|\alpha|^2 + (1-p)|\beta|^2]}$, which can be calculated using Eqs. (15)–(17):

$$F_{\text{av,n}} = \frac{1}{2} + \frac{\sqrt{1-p}(2-p) - 2(1-p)}{p^2} + \frac{(1-p)(2\sqrt{1-p} - 2 + p)}{p^3} \ln(1-p) \quad (21)$$

For $p \ll 1$ this gives $F_{\text{av,n}} \approx 1 - p^2/24$, showing a slow, quadratic in time decrease of fidelity in the no-relaxation scenario in contrast to the linear decrease (19) of the fidelity averaged over both scenarios. Therefore our gedanken experiment could be used for quantum error detection: if no relaxation is recorded, we know that the initial state is well-preserved at short times.

Note that we have averaged the state fidelities $F_{\text{st,r}}$ and $F_{\text{st,n}}$ over the Bloch sphere with uniform weight, as in the standard definition [2, 27] of the averaged state fidelity. Another meaningful averaging is using weights proportional to the probabilities of the corresponding scenarios. [This would correspond to an equal number of experimental runs for each point of a uniform mesh on the Bloch sphere, as opposed to an equal number of “successful” (i.e. selected) runs for the previous definition.] Thus defined average fidelities are

$$\tilde{F}_{\text{av,r}} = \overline{|\alpha|^2 P_r / \overline{P_r}} = 1/3, \quad (22)$$

$$\tilde{F}_{\text{av,n}} = \overline{(|\alpha|^2 + \sqrt{1-p}|\beta|^2)^2 / \overline{P_n}} = \frac{2-p + \sqrt{1-p}}{3-3p/2}, \quad (23)$$

where $\overline{P_r} = p/2$ and $\overline{P_n} = 1 - p/2$ are the averaged probabilities of the two scenarios. The advantage of this definition is a natural formula for the non-selected average fidelity:

$$F_{\text{av}} = \tilde{F}_{\text{av,r}} \overline{P_r} + \tilde{F}_{\text{av,n}} \overline{P_n} \quad (24)$$

[see Eq. (7)]. In this paper when discussing selected scenarios (as for QED) we will use both ways to average

over the Bloch sphere. Note that $\tilde{F}_{\text{av,n}} \approx 1 - p^2/24$ for $p \ll 1$, which is the same as for $F_{\text{av,n}}$ ($\tilde{F}_{\text{av,n}}$ and $F_{\text{av,n}}$ are practically indistinguishable at $p \lesssim 1/2$), indicating that the difference between the two definitions is not very significant in the cases that are of most interest for this paper.

B. Two-qubit encoding

Let us use the procedure of Fig. 1 with only one ancilla qubit. The encoded state is then $\alpha|00\rangle + \beta|11\rangle$. The state evolution due to energy relaxation can be unraveled into four scenarios: no relaxation, relaxation in either the first (main) or second (ancilla) qubit, and relaxation in both qubits. The corresponding wavefunctions and probabilities after time t of energy relaxation are

$$\left\{ \begin{array}{l} \frac{\alpha|00\rangle + \beta\sqrt{1-p_1}\sqrt{1-p_2}|11\rangle}{\sqrt{P_{\text{nn}}}}, \\ |01\rangle, \text{ prob. } P_{\text{rn}} = |\alpha|^2 + |\beta|^2 (1-p_1)(1-p_2), \\ |10\rangle, \text{ prob. } P_{\text{nr}} = |\beta|^2 (1-p_1)p_2, \\ |00\rangle, \text{ prob. } P_{\text{rr}} = |\beta|^2 p_1p_2, \end{array} \right. \quad (25)$$

where

$$p_1 = 1 - e^{-t/T_1^{(1)}}, \quad p_2 = 1 - e^{-t/T_1^{(2)}} \quad (26)$$

are the single-qubit probabilities of relaxation from the excited state $|1\rangle$. This simple unraveling is possible because the energy relaxation occurs only in component $|11\rangle$ of the superposition, and in this component the qubits are unentangled. This is why the probabilities of the scenarios are the simple products of individual probabilities. The validity of Eq. (25) can also be checked by considering particular time moments at which the relaxation events happen and integrating over these moments; this is a more direct but more cumbersome way.

After the decoding procedure consisting of one CNOT operation, the two-qubit state is a product-state in all four scenarios:

$$\left\{ \begin{array}{l} \frac{\alpha|0\rangle + \beta\sqrt{1-p_1}\sqrt{1-p_2}|1\rangle}{\sqrt{P_{\text{nn}}}} \otimes |0\rangle, \text{ prob. } P_{\text{nn}}, \\ |01\rangle, \text{ prob. } P_{\text{rn}}, \\ |11\rangle, \text{ prob. } P_{\text{nr}}, \\ |00\rangle, \text{ prob. } P_{\text{rr}}, \end{array} \right. \quad (27)$$

with a definite result of the ancilla qubit measurement in each scenario. The state of the main qubit is different from the initial state $|\psi_{\text{in}}\rangle$ in all four scenarios, and the corresponding state fidelities are $[|\alpha|^2 + |\beta|^2\sqrt{1-p_1}\sqrt{1-p_2}]^2/P_{\text{nn}}$, $|\alpha|^2$, $|\beta|^2$, and $|\alpha|^2$.

As discussed above, we consider three ways to proceed: ignore the measurement result, select only result 0, or try to correct the main qubit state. If the measurement result is ignored, then all four scenarios are added up and

the average fidelity is

$$F_{\text{av}}^{\text{ign}} = \frac{[|\alpha|^2 + |\beta|^2 \sqrt{1-p_1} \sqrt{1-p_2}]^2}{+|\alpha|^2 P_{\text{rn}} + |\beta|^2 P_{\text{nr}} + |\alpha|^2 P_{\text{rr}}}, \quad (28)$$

where the averaging is over the Bloch sphere. Using the formulas for the probabilities from Eq. (25) and the averages $\overline{|\alpha|^2}$, $\overline{|\beta|^2}$, $\overline{|\alpha|^4}$, $\overline{|\beta|^4}$, and $\overline{|\alpha|^2|\beta|^2}$ from Eqs. (9)–(11), we obtain

$$F_{\text{av}}^{\text{ign}} = \frac{2}{3} + \frac{\sqrt{(1-p_1)(1-p_2)}}{3} - \frac{p_1}{6} \quad (29)$$

For small $p_{1,2}$ (at short time t) it is $F_{\text{av}}^{\text{ign}} \approx 1 - p_1/3 - p_2/6$, and it is obviously worse than the case without encoding/decoding of the main qubit – see Eqs. (18) and (19). Note that Eq. (29) can also be obtained by averaging the state fidelity only over the 6 initial states (see Appendix).

In quantum error detection we consider ancilla measurement result 1 as an error and select only the cases when the measurement gives 0. This selects scenarios with either no relaxation or two relaxation events [see the first and last lines of Eq. (27)]. The averaged (with uniform weight) state fidelity in this case is

$$F_{\text{av}}^{\text{qed}} = \frac{[|\alpha|^2 + |\beta|^2 \sqrt{1-p_1} \sqrt{1-p_2}]^2 + |\alpha|^2 P_{\text{rr}}}{P_{\text{nn}} + P_{\text{rr}}} \quad (30)$$

(the fraction is averaged over the Bloch sphere), which can be calculated using Eqs. (15)–(17):

$$F_{\text{av}}^{\text{qed}} = \frac{1}{2} + \frac{s-1}{B} + \frac{p_1 + p_2 - 2 + 2s}{B^2} + \frac{(1+B)^2 + s^2 - (1+B)(2s + p_1 p_2)}{B^3} \ln(1+B), \quad (31)$$

where $B = 2p_1 p_2 - p_1 - p_2$ and $s = \sqrt{1-p_1} \sqrt{1-p_2}$. For the small-error case (at short time t) this gives

$$F_{\text{av}}^{\text{qed}} \approx 1 - (p_1^2 + p_2^2)/24 - 5p_1 p_2/12, \quad p_{1,2} \ll 1. \quad (32)$$

If we use the averaging over the Bloch sphere with weight proportional to the probability $P_{\text{nn}} + P_{\text{rr}}$ of the measurement result 0, then

$$\tilde{F}_{\text{av}}^{\text{qed}} = \frac{[|\alpha|^2 + |\beta|^2 \sqrt{1-p_1} \sqrt{1-p_2}]^2 + |\alpha|^2 P_{\text{rr}}}{P_{\text{nn}} + P_{\text{rr}}}, \quad (33)$$

(the numerator and denominator are averaged separately), which gives

$$\tilde{F}_{\text{av}}^{\text{qed}} = \frac{2 - p_1 - p_2 + \frac{3}{2} p_1 p_2 + \sqrt{1-p_1} \sqrt{1-p_2}}{3[1 + p_1 p_2 - (p_1 + p_2)/2]}. \quad (34)$$

[Note that instead of using Eqs. (9)–(11), the 6-point averaging trick can be used separately for the numerator and denominator of Eq. (33) – see Appendix.] At short times this gives $\tilde{F}_{\text{av}}^{\text{qed}} \approx 1 - (p_1^2 + p_2^2)/24 - 5p_1 p_2/12$, same as for $F_{\text{av}}^{\text{qed}}$ [see Eq. (32)].

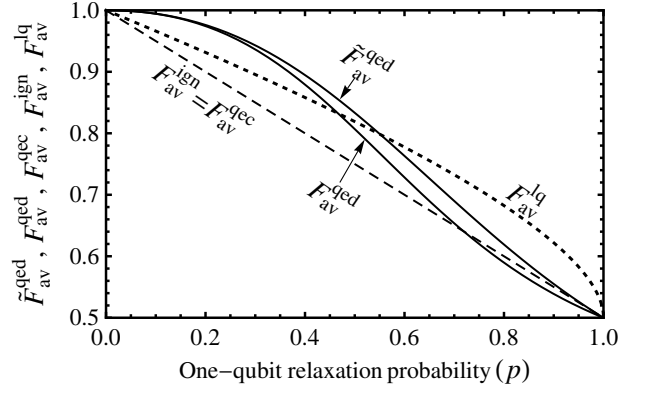


FIG. 2: Average state preservation fidelities for the two-qubit encoding (compared with no encoding), as functions of the one-qubit energy relaxation probability $p = 1 - e^{-t/T_1}$ (same for both qubits, $p_1 = p_2 = p$). The solid lines show the QED fidelities $F_{\text{av}}^{\text{qed}}$ and $\tilde{F}_{\text{av}}^{\text{qed}}$ given by Eqs. (31) and (34). ($F_{\text{av}}^{\text{qed}}$ assumes averaging over the Bloch sphere with uniform weight, while for $\tilde{F}_{\text{av}}^{\text{qed}}$ the weight is proportional to the probability of the “no error” measurement result 0.) The dashed line shows the QEC fidelity $F_{\text{av}}^{\text{qec}}$, which coincides with $F_{\text{av}}^{\text{ign}}$, for which the measurement result is ignored, Eqs. (29) and (35). The dotted line shows the one-qubit fidelity $F_{\text{av}}^{\text{1q}}$ without encoding, Eq. (18). QEC performs worse than no encoding, while QED provides a significant improvement for $p \lesssim 0.3$.

Figure 2 shows the QED fidelity defined in both ways, $F_{\text{av}}^{\text{qed}}$ and $\tilde{F}_{\text{av}}^{\text{qed}}$, as functions of the one-qubit relaxation probability, assuming similar qubits, $p_1 = p_2 = p$. For $p \lesssim 0.3$ both fidelities are significantly higher than the fidelity $F_{\text{av}}^{\text{1q}}$ for an unencoded single qubit [given by Eq. (18)], which itself is higher than the fidelity $F_{\text{av}}^{\text{ign}}$ when the ancilla measurement result is ignored [Eq. (29)].

Now let us discuss whether or not the state of the main qubit can be made closer to $|\psi_{\text{in}}\rangle$ using the measurement result information, as in quantum error correction. If the measurement result is 0, then the qubit state is described by the first and last lines of Eq. (27). It is rather obvious that in this case no unitary operation can improve further the average fidelity [for QEC we are interested in averaging with the weight proportional to probability – see Eq. (24)]. This statement is rigorously proven in the Appendix. So, no correction should be applied for measurement result 0. (Actually, a non-unitary operation due to partial collapse can increase the fidelity in this case [29–32], but we consider only unitary operations, as it should be in the usual QEC.) When the measurement result is 1, the main qubit is in the state $|0\rangle$ with probability $P_{\text{rn}}/(P_{\text{rn}} + P_{\text{nr}})$ or in the state $|1\rangle$ with remaining probability $P_{\text{nr}}/(P_{\text{rn}} + P_{\text{nr}})$ – see Eq. (27). In the case $p_1 = p_2$ this is the fully mixed state, and any unitary operation does not change it. Thus a meaningful error correction is impossible, and therefore $F_{\text{av}}^{\text{qec}} = F_{\text{av}}^{\text{ign}}$ (see Fig. 2).

Actually, if $p_2 > p_1$, then a slight improvement of fidelity is possible by applying the π -pulse (exchanging

states $|0\rangle$ and $|1\rangle$) when the measurement result is 1. This makes the resulting state closer to $|1\rangle$ than to $|0\rangle$, and correspondingly on average closer to $|\psi_{\text{in}}\rangle$, because the probability of measuring 1 increases with $|\psi_{\text{in}}\rangle$ being closer to $|1\rangle$. The optimality of this procedure for measurement result 1 is proven in the Appendix. It is easy to calculate the fidelity change due to the π -pulse (the easiest way is to average over the 6 initial states and to work with unnormalized states – see Appendix). The resulting optimal QEC fidelity for the 2-qubit encoding of Fig. 1 is

$$F_{\text{av}}^{\text{qec}} = \frac{2}{3} + \frac{\sqrt{(1-p_1)(1-p_2)}}{3} - \frac{\min(p_1, p_2)}{6}. \quad (35)$$

C. N -qubit encoding

We now extend our discussion of the protocol of Fig. 1, including $N-1$ ancilla qubits. The encoded state is then $\alpha|0^N\rangle + \beta|1^N\rangle$. The state evolution can be unraveled into 2^N scenarios depending on which qubits relax. However, there are 2^{N-1} measurement results, and each of them corresponds to two scenarios. If the main qubit does not relax, then the measurement result directly shows which ancilla qubits relax (i.e. result 1 indicates the relaxation event), while if the main qubit relaxes, then the relaxation scenario is shown by the complement of the measurement result (i.e. result 0 indicates relaxation).

The measurement result $\mathbf{0}$ (all zeros) indicates that the main qubit is either in the state

$$|\psi_{\text{none}}\rangle = \frac{1}{\sqrt{P_{\text{none}}}} \left(\alpha|0\rangle + \beta|1\rangle \prod_{j=1}^N \sqrt{1-p_j} \right), \quad (36)$$

where $P_{\text{none}} = |\alpha|^2 + |\beta|^2 \prod_{j=1}^N (1-p_j)$ is the probability that no qubits relax, or in the state $|0\rangle$ if all qubits relax, with the corresponding probability $P_{\text{all}} = |\beta|^2 \prod_{j=1}^N p_j$. For any other measurement result the main qubit is either in state $|0\rangle$ or $|1\rangle$, with easily calculable probabilities of the scenarios. For simplicity we assume $p_j = p$ below.

As in the previous subsection, we consider three possible ways to proceed: ignore the measurement result, select only cases with measurement result $\mathbf{0}$ (QED), or try to improve the fidelity when an error is detected (QEC). If the measurement result is ignored, the average fidelity (calculated in a similar way as above) is

$$F_{\text{av}}^{\text{ign}} = \frac{2}{3} + \frac{(1-p)^{N/2}}{3} - \frac{p}{6}; \quad (37)$$

it obviously decreases with increasing number of ancilla qubits.

In quantum error detection we select only cases with measurement result $\mathbf{0}$. Then the state fidelity is

$$F_{\text{st}}^{\text{qed}} = \frac{(|\alpha|^2 + |\beta|^2(1-p)^{N/2})^2 + |\alpha|^2 P_{\text{all}}}{P_{\text{none}} + P_{\text{all}}}, \quad (38)$$

and averaging it over the Bloch sphere with uniform weight we obtain

$$F_{\text{av}}^{\text{qed}} = \frac{-3 + S + (1-p)^N}{2B} + \frac{-1 + S - (1-p)^N}{B^2} + \frac{(1+B)^2 + (1-p)^N - S(1+B)}{B^3} \ln(1+B), \quad (39)$$

where $B = -1 + (1-p)^N + p^N$ and $S = 2(1-p)^{N/2} + p^N$. For $N=2$ this equation corresponds to Eq. (31). The small-error approximation for $N \geq 3$ is

$$F_{\text{av}}^{\text{qed}} \approx 1 - N^2 p^2 / 24, \quad p \ll 1. \quad (40)$$

It is interesting to note that this approximation does not work for $N=2$, for which $F_{\text{av}}^{\text{qed}} \approx 1 - p^2/2$, as follows from Eq. (32). The reason is that P_{all} scales as p^N , and therefore for $N \geq 3$ Eq. (40) does not have a quadratic contribution from the scenario when all qubits relax; the infidelity comes only from the difference between $|\psi_{\text{none}}\rangle$ and $|\psi_{\text{in}}\rangle$. In contrast, for $N=2$ the fidelity $F_{\text{av}}^{\text{qed}}$ is further decreased by $p^2/3$ due to relaxation of both qubits.

From Eqs. (40) and (32) we see that the best QED fidelity in the small-error case ($p \ll 1$) is achieved by the 3-qubit encoding, $N=3$; then $1 - F_{\text{av}}^{\text{qed}} \approx (3/8)p^2$. However, this is only the factor 4/3 better (smaller) than for $N=2$. Therefore, from the experimental point of view the 2-qubit encoding (which is easier to realize than the 3-qubit encoding) seems to be most natural.

If we use the averaging of the QED state fidelity (38) with weights proportional to the probability $P_{\text{none}} + P_{\text{all}}$ of the measurement result $\mathbf{0}$, then we essentially need to average the numerator and denominator of Eq. (38) separately, thus obtaining

$$\tilde{F}_{\text{av}}^{\text{qed}} = \frac{2}{3} \frac{1 + (1-p)^N + (1-p)^{N/2} + \frac{1}{2}p^N}{1 + (1-p)^N + p^N}. \quad (41)$$

In the small-error case ($p \ll 1$) for $N \geq 3$ this gives $\tilde{F}_{\text{av}}^{\text{qed}} \approx 1 - N^2 p^2 / 24$, same as Eq. (40) for $F_{\text{av}}^{\text{qed}}$.

Figure 3(a) shows the QED fidelities $F_{\text{av}}^{\text{qed}}$ and $\tilde{F}_{\text{av}}^{\text{qed}}$ for $N=2, 3$, and 4. We see that the difference between $F_{\text{av}}^{\text{qed}}$ and $\tilde{F}_{\text{av}}^{\text{qed}}$ becomes larger with increasing N , but the difference is small at small p . Note that the QED fidelity for the 2-qubit encoding becomes better than for the 3-qubit encoding for $p \gtrsim 0.3$.

Now let us discuss the possibility of QEC protocols, which use unitary correcting operations depending on the measurement result. If the result is $\mathbf{0}$, then the unnormalized density matrix of the main qubit is $P_{\text{none}}|\psi_{\text{none}}\rangle\langle\psi_{\text{none}}| + P_{\text{all}}|0\rangle\langle 0|$. As proven in the Appendix, no unitary operation can increase the fidelity in this case (in contrast to non-unitary partial-collapse operations [29–32]). For all other measurement results, the main qubit is in the incoherent mixture of the states $|0\rangle$ and $|1\rangle$; the unnormalized density matrix is $P_{0,m}|0\rangle\langle 0| + P_{1,m}|1\rangle\langle 1|$, where the corresponding probabilities are $P_{1,m} = |\beta|^2(1-p) \prod_{i=2,N} f(m_i)$ and $P_{0,m} =$

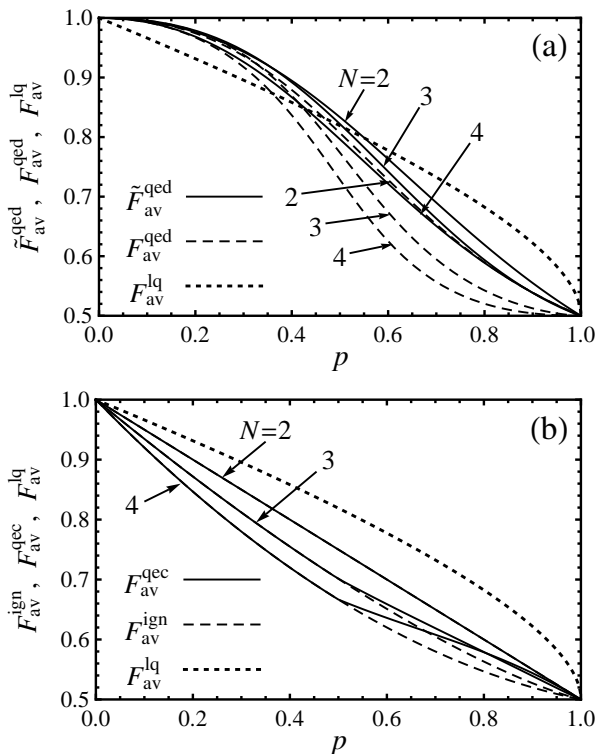


FIG. 3: (a) The QED fidelities \tilde{F}_{av}^{qed} (solid lines) and F_{av}^{qed} (dashed lines) for the encoding using $N = 2, 3$, and 4 physical qubits, as functions of the single-qubit energy relaxation probability p . The dotted line shows the fidelity F_{av}^{lq} for an unencoded qubit. (b) The optimal QEC fidelity F_{av}^{qec} (solid lines) and the fidelity F_{av}^{ign} when the measurement result is ignored (dashed lines) for $N = 2, 3$, and 4.

$|\beta|^2 p \prod_{i=2, N} f(1 - m_i)$, where $f(1) = p$, $f(0) = 1 - p$, and m_i is the measurement result for the i th ancilla qubit. As shown in the Appendix, the maximum fidelity is then achieved by applying the π -pulse (exchanging $|0\rangle$ and $|1\rangle$) if $P_{1,m} < P_{0,m}$ and doing nothing if $P_{1,m} \geq P_{0,m}$. Calculating the corresponding qubit state fidelity (compared with the initial state), summing over the 2^{N-1} measurement results, and averaging over the Bloch sphere, we obtain the QEC fidelity

$$F_{av}^{qec} = \frac{1}{2} + \frac{1}{3}(1-p)^{N/2} + \frac{1}{6}(1-p)^N + \frac{1}{6} \max[p - p^N, (1-p) - (1-p)^N]. \quad (42)$$

The QEC fidelity as well as the fidelity F_{av}^{ign} for ignoring the measurement result are shown in Fig. 3(b) for $N = 2, 3$, and 4. The curves for F_{av}^{qec} and F_{av}^{ign} coincide at $p \leq 1/2$, because in this case the optimal correction is no correction. We see that for any N the QEC fidelity is smaller than the no-encoding fidelity F_{av}^{lq} , so the error correction by a repetitive code does not protect against energy relaxation.

D. Discussion

Our results show that the repetitive codes do not work for QEC protection against energy relaxation. This is because energy relaxation is very different from a bit flip (or phase flip or bit-phase flip), for which repetitive codes work well. In the language of quantum stabilizer codes [2] the event of energy relaxation corresponds to the “sum” of two errors: bit flip (X -operation) and bit-phase flip (Y -operation) – see the Kraus operator A_r in Eq. (5). So, a stabilizer code should be able to protect against both of these errors to protect against energy relaxation events. [Actually, a weaker error due to the “no relaxation” Kraus operator A_r in Eq. (5) also requires protection against phase flip (Z -operation) errors.] For example, the standard 5-qubit and 7-qubit QEC codes [1, 2, 24] protect against all 3 types of errors (X, Y, Z), and therefore can protect against energy relaxation.

Using the approach of the stabilizer codes and the quantum Hamming bound [2], let us calculate the minimum number of qubits N to protect against X and Y errors. The Hilbert space of the dimension 2^N can be divided into 2^{N-1} orthogonal two-dimensional subspaces (“copies” of the qubit space); these subspaces should be able to distinguish the cases with various errors and no error. Since the number of possible errors is $2N$, we have an inequality $2^{N-1} \geq 1 + 2N$. From this inequality we find $N \geq 5$ (the same minimum as for all 3 types of quantum errors). Notice, however, that an approximate QEC for energy relaxation is possible for $N = 4$ [33] (see also [34]). This code breaks the above limitation because the relaxation event is treated as one error, not as a “sum” of X and Y (the drawback though is a slightly probabilistic operation). In any case, the QEC codes protecting against energy relaxation are much more complicated than the repetitive codes.

Even though the repetitive codes are not good for QEC protection against energy relaxation, we have shown that they can be well used for QED. Moreover, only 2-qubit encoding is sufficient for that. An interesting question is whether or not it is beneficial to do many cycles of QED, correspondingly decreasing the time of each cycle and therefore the error probability p in each cycle (such division into shorter cycles is beneficial for QEC [1, 2]). The simple answer is that such division into shorter cycles does not help much for the protocol of Fig. 1. The reason is that even when no relaxation events happen, the qubit state changes – see Eq. (36), because the absence of relaxation preferentially indicates state $|0\rangle$ and plays the same role as the partial collapse [30]. Rewriting Eq. (36) in a non-normalized way as $|\psi_{\text{none}}\rangle = \alpha|0\rangle + \beta|1\rangle \prod_{j=1}^N \exp(-t/2T_{1,j})$, we see that division into several QED cycles does not change the final wavefunction $|\psi_{\text{none}}\rangle$ as long as the total time t is the same. Therefore, since for $N \geq 3$ this evolution is the main reason for imperfect QED fidelity at $p \ll 1$ (see discussion in the previous subsection), there is not much benefit of using the QED cycles. Nevertheless, some im-

provement of the QED fidelity will be due to a decrease of the probability P_{all} that all qubits relax. Since this probability scales as $p^N \approx (t/T_1)^N$, the division into M cycles is expected to decrease the corresponding contribution to the procedure infidelity by the factor M^{N-1} . This improvement will be most significant for $N = 2$: it will essentially change the approximation $F_{\text{av}}^{\text{qed}} \approx 1 - p^2/2$ given by Eq. (32) into $F_{\text{av}}^{\text{qed}} \approx 1 - p^2/6$ given by Eq. (40) for $N = 2$.

A more important improvement of the QED fidelity can be achieved if the no-relaxation evolution (36) of $|\psi_{\text{none}}\rangle$ is compensated. One way is to apply a partial measurement [29–31] to the main qubit after the procedure, essentially eliminating the evolution (36) for the price of a further decrease of the selection probability (probability of success). Another, easier way is to apply π -pulses, exchanging states $|0\rangle$ and $|1\rangle$, between (after) the QED cycles (these π -rotations can be around any axis in the equatorial plane of the Bloch sphere). Then for an even number of equal-duration QED cycles, the no-relaxation evolution (36) will be compensated exactly (as in the uncollapsing procedure [29, 31, 32, 35]), and the QED infidelity $1 - F^{\text{qed}}$ will be only due to the contribution from P_{all} . (The use of π -pulses resembles dynamical decoupling of the “bang-bang” type [36]; however, the resemblance is accidental, since dynamical decoupling cannot protect against the energy relaxation [37].)

For an estimate of the corresponding QED fidelity, let us consider the procedure with total duration $t \lesssim T_1$, divided into M cycles of duration t/M each (M is even). In each cycle $p \approx t/MT_1 \ll 1$, and if we assume $Nt/MT_1 \ll 1$, then $|\psi_{\text{none}}\rangle \approx |\psi_{\text{in}}\rangle$ in Eq. (36). The probability that the N -qubit relaxation (which remains undetected) happened in the first cycle is $P_{\text{all}} = |\beta|^2 p^N$, and similar probability for the second cycle (after π -pulse) is $|\alpha|^2 p^N$. Therefore, in a selected QED realization (with all measurement results $\mathbf{0}$) the probability to have an undetected relaxation event is $(M/2)p^N$, independent of the initial state (we assume this probability to be small, then we can neglect the double-events). If such an undetected relaxation event happens, then the average fidelity is $\tilde{F}_{\text{av}} = \overline{|\alpha|^2 |\beta|^2} / \overline{|\alpha|^2} = 1/3$. The QED fidelity then can be calculated as $1 - (1 - 1/3) \times (M/2)p^N$, which gives

$$F_{\text{av}}^{\text{qed}} \approx \tilde{F}_{\text{av}}^{\text{qed}} \approx 1 - M(t/MT_1)^N/3. \quad (43)$$

(If the above assumption $Nt/MT_1 \ll 1$ is violated, then the factor $1/3$ changes, but the scaling remains the same.) We see that for this procedure the division into a larger number of cycles M is beneficial, as well as using more qubits (N) for the encoding. Note that our QED procedure does not prevent the relaxation events from happening, so the average probability of observing the “no error” result $\mathbf{0}$ in all M cycles is approximately $\exp(-tN/2T_1)$.

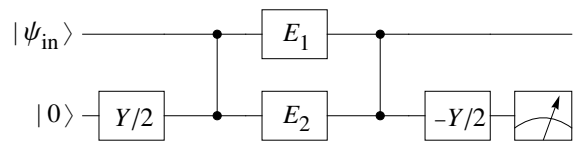


FIG. 4: Two-qubit experimental protocol for realizing quantum error detection/correction. Notations E_1 and E_2 represent the four detectable error rotations: $R_1^X(2\theta)$, $R_1^Y(2\theta)$, $R_2^Y(2\theta)$, and $R_2^Z(2\theta)$. Notations $Y/2$ and $-Y/2$ represent $R^Y(\pi/2)$ and $R^Y(-\pi/2)$, respectively.

III. TWO-QUBIT ERROR DETECTION AND CORRECTION FOR PHASE QUBITS

In this section we propose and analyze the operation of two-qubit error detection/correction protocols designed for experimental implementation with the current technology of superconducting phase qubits. We will discuss several similar protocols (including the QED protocol for energy relaxation); for all of them the goal is to preserve an arbitrary initial state $|\psi_{\text{in}}\rangle = \alpha|0\rangle + \beta|1\rangle$ of a qubit.

The first procedure (which we will mostly consider) is shown in Fig. 4; it is designed to preserve the state $|\psi_{\text{in}}\rangle$ of the upper (main) qubit. Encoding is performed by preparing the lower (ancilla) qubit in the state $(|0\rangle + |1\rangle)/\sqrt{2}$ by starting with the ground state $|0\rangle$ and using the Y -rotation over the angle $\pi/2$ (denoted as $Y/2$), and then applying the controlled- Z (CZ) gate between the two qubits. [Note that the CZ gate is the natural entangling operation for the phase qubits [19, 23, 38].] This produces the entangled two-qubit wavefunction

$$[\alpha|0\rangle \otimes (|0\rangle + |1\rangle) + \beta|1\rangle \otimes (|0\rangle - |1\rangle)]/\sqrt{2}, \quad (44)$$

where the leftmost entry represents the main qubit. After encoding, the decoherence process is simulated by applying a unitary rotation to one of the qubits. For this encoding we consider a set of four possible rotations: $R_1^X(2\theta)$, $R_1^Y(2\theta)$, $R_2^Y(2\theta)$, and $R_2^Z(2\theta)$, where the subscript indicates the qubit number (1 for the main qubit), the superscript is the rotation axis on the Bloch sphere, and the argument 2θ is the rotation angle on the Bloch sphere (the corresponding rotation angle in the wavefunction language is θ).

After the error rotation has been applied, the resultant state is decoded by inverting the encoding operation, and the ancilla qubit is measured in the computational basis. In the absence of error rotation, the state after decoding is $(\alpha|0\rangle + \beta|1\rangle) \otimes |0\rangle$, so that the initial state of the main qubit is restored and the measurement result for the ancilla qubit is 0. The error rotation disturbs the final state, which probabilistically changes the measurement result to 1 and also changes the final state of the main qubit.

A. Analysis of the ideal case

Let us start with analyzing the effect of the error rotation $R_1^X(2\theta)$ (X -rotation of the main qubit). It transforms the encoded state (44) into the state

$$[\alpha(\cos\theta|0\rangle - i\sin\theta|1\rangle) \otimes (|0\rangle + |1\rangle) + \beta(-i\sin\theta|0\rangle + \cos\theta|1\rangle) \otimes (|0\rangle - |1\rangle)]/\sqrt{2}, \quad (45)$$

which after decoding (but before measurement) becomes

$$\cos\theta|\psi_{\text{in}}\rangle|0\rangle + i\sin\theta X|\psi_{\text{in}}\rangle|1\rangle, \quad (46)$$

where X is the Pauli- X -matrix transformation [2]. It is clear that we obtain ancilla measurement result 0 with probability $\cos^2\theta$, and then the state of the main qubit is restored to $|\psi_{\text{in}}\rangle$, or obtain result 1 with probability $\sin^2\theta$, which leaves the main qubit in the state $X|\psi_{\text{in}}\rangle$. [In this section we use the standard quantum computing notations [2], in which the Pauli matrices act on column vectors with the upper element corresponding to the state $|0\rangle$. Note that for one-qubit wavefunctions $R^X(\pi) = -iX$.]

In quantum error detection we select only result 0, and this gives the perfect state preservation fidelity, $F_{\text{st}}^{\text{qed}} = 1$, for any initial state. We can also use the approach of quantum error correction and apply the X gate [i.e. $R^X(\pi)$] to the main qubit when the error result 1 is measured. This produces the initial state $|\psi_{\text{in}}\rangle$ for both measurement results with perfect fidelity, $F_{\text{st}}^{\text{qec}} = 1$. Therefore, the QED and QEC fidelities averaged over the Bloch sphere are also perfect,

$$F_{\text{av}}^{\text{qed}} = F_{\text{av}}^{\text{qec}} = 1. \quad (47)$$

Notice, however, that for QEC we had to know that an error is due to the X -rotation applied to the first qubit. This is different from “real” error correction, in which we do not know the type of error, but is acceptable for a demonstration experiment.

Let us also calculate the storage fidelity if the measurement result is ignored (or, equivalently, the ancilla qubit is not measured). From Eq. (46) we obtain the state fidelity for the main qubit $F_{\text{st}}^{\text{ign}} = \cos^2\theta + \sin^2\theta \langle \psi_{\text{in}} | X | \psi_{\text{in}} \rangle^2$, which after averaging over the Bloch sphere becomes

$$F_{\text{av}}^{\text{ign}} = \cos^2\theta + (\sin^2\theta)/3. \quad (48)$$

Note that if the rotation $R^X(2\theta)$ is applied to a qubit without encoding, then the average fidelity is still given by Eq. (48), so the encoding with ignored measurement result (or no measurement) does not affect the average preservation fidelity (moreover, it does not affect the state fidelity for any initial state).

Now let us analyze in a similar way the case when the error is introduced by the Y -rotation of the main qubit, $R_1^Y(2\theta)$. Then the two-qubit state before the measurement is

$$\cos\theta|\psi_{\text{in}}\rangle|0\rangle + i\sin\theta Y|\psi_{\text{in}}\rangle|1\rangle, \quad (49)$$

so that the measurement result 0 still restores the initial state $|\psi_{\text{in}}\rangle$ of the main qubit, while for the measurement result 1 the state of the main qubit is $Y|\psi_{\text{in}}\rangle$, thus requiring the Y -gate correction [i.e. $R^Y(\pi) = -iY$]. The QED and QEC fidelities are still perfect, Eq. (47), while the fidelity with ignored result is still given by Eq. (48). Note that the correcting Y -gate is different from the correcting X -gate in the previous case, so we need to know the type of the error to apply the proper correction (in a demonstration experiment the error rotation is applied intentionally, so its type is obviously known).

Now let us consider the error due to the Y -rotation of the ancilla qubit, $R_2^Y(2\theta)$. Then the state before the measurement is

$$\cos\theta|\psi_{\text{in}}\rangle|0\rangle + \sin\theta Z|\psi_{\text{in}}\rangle|1\rangle, \quad (50)$$

and therefore in the case of measurement result 1 the Z -gate correction is needed to restore $|\psi_{\text{in}}\rangle$, while for the measurement result 0 no correction is needed. Equations (47) and (48) are still valid.

Finally, for the Z -rotation of the ancilla qubit, $R_2^Z(2\theta)$, the state before the measurement is

$$|\psi_{\text{in}}\rangle(\cos\theta|0\rangle + i\sin\theta|1\rangle). \quad (51)$$

The final state of the main qubit is insensitive to this rotation, and therefore no correction is needed for both measurement results. In this case Eq. (47) is still valid, while Eq. (48) is replaced by $F_{\text{av}}^{\text{ign}} = 1$.

We have discussed the effect of four error rotations: $R_1^X(2\theta)$, $R_1^Y(2\theta)$, $R_2^Y(2\theta)$, and $R_2^Z(2\theta)$. The two remaining rotations, $R_1^Z(2\theta)$ and $R_2^X(2\theta)$, gradually change the final state of the main qubit (both produce its Z -rotations) but always produce final state $|0\rangle$ of the ancilla qubit. Therefore, these errors are undetectable and are excluded from our set of error rotations.

As discussed above, for QEC we need to know which one out of four error types has been applied. In contrast, for QED we do not need to know the error type; for all of them the measurement result 0 indicates the perfect state of the main qubit. Moreover, for QED these types of error rotations can be applied simultaneously, as long as the rotation angles are relatively small, to make negligible the second-order terms (which in the QEC/QED language correspond to double-errors).

It is most natural to view the analyzed procedure as a QED protocol. However, we would like to emphasize that its interpretation as a QEC protocol is also possible: the proper correction is possible when we know which error process is applied. (In the existing QEC experiments the types of allowed errors are almost always limited; in our protocol the number of allowed types is further reduced to one out of four.) Most importantly, our simple two-qubit protocol demonstrates the main “miracle” of QEC, that continuous quantum errors can be transformed into discrete errors, and then corrected.

B. Realization using phase qubits

So far we considered the ideal case when there is no physical decoherence of qubits, and the loss of fidelity is only due to intentional rotations of the qubit states. In this subsection we discuss a more realistic experimental situation, with added decoherence during the protocol. We will have in mind the present-day technology of superconducting phase qubits [19, 23, 38].

Note that the phase qubit technology provides a high-fidelity measurement (about 95% [19], so we consider it perfect in the simulations); however, it takes a significant time to read out the measurement result (longer than the qubit decoherence time). While this is not a problem for the QED, the QEC at present cannot be done in real time. Nevertheless, there is a simple way to go around this difficulty in an experiment. The resulting state of the main qubit is measured by using the quantum state tomography (QST), so the experiment is necessarily repeated many times. It is easy to separate the QST data for ancilla measurement results 0 and 1. In this way two different density matrices of the main qubit are obtained for ancilla measurement 0 and 1. For the result 1 it is then easy to calculate the density matrix after the correcting operation (if it were applied in real time). Finally adding the two density matrices (with weights equal to the probabilities of ancilla measurement results), the qubit density matrix for the QEC procedure is obtained.

In phase qubits [19, 23, 38] the main sources of decoherence are single-qubit energy relaxation (with T_1 on the order of $0.5 \mu\text{s}$) and pure dephasing (with a comparable or a little shorter dephasing time T_φ). The decoherence is somewhat reduced in the RezQu architecture [23, 26], in which the quantum information is often transferred between the phase qubits and resonators (resonators have much longer T_1 and practically no pure dephasing). We have simulated the procedure of Fig. 4 in a simplified way, which does not explicitly reproduce the RezQu implementation of the protocol, but still uses a reasonable account of realistic decoherence.

For simplicity for each qubit we assume $T_1 = T_2$ (so that the pure dephasing time is $T_\varphi = 2T_1$). We assume that single-qubit rotations [including $R^Y(\pm\pi/2)$ of ancilla qubit, preparation of the main qubit, and error rotations] take 10 ns each, CZ gates take 40 ns each, and there are 5 ns spacings between the operations. Then the whole protocol of Fig. 4 (ending before measurement of ancilla qubit and tomography of the main qubit) takes 135 ns. We calculate the evolution of the two-qubit density matrix by breaking the procedure into small time steps and applying energy relaxation and pure dephasing to each qubit (for simplicity the CZ gate is simulated as a gradual accumulation of the phase, as would be for the dispersive gate). We start with 6 initial states of the main qubit $[|0\rangle, |1\rangle, (|0\rangle \pm |1\rangle)/\sqrt{2}, (|0\rangle \pm i|1\rangle)/\sqrt{2}]$, labeled by index $j = 1, \dots, 6$ below], and from the final two-qubit density matrices we calculate reduced unnormalized one-qubit density matrices $\rho_{0,j}$ and $\rho_{1,j}$, corresponding to

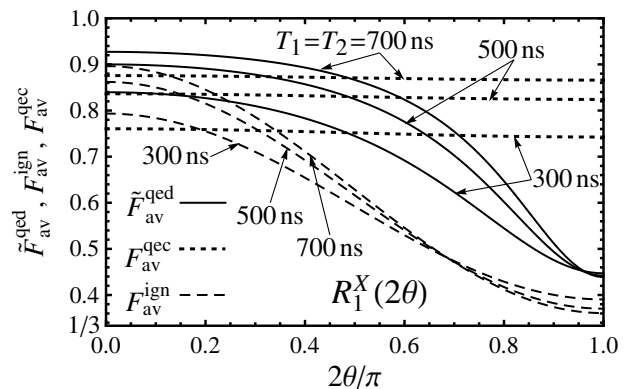


FIG. 5: Numerical results for the average QED fidelity $\tilde{F}_{\text{av}}^{\text{qec}}$ (solid lines), the QEC fidelity $F_{\text{av}}^{\text{qec}}$ (dotted lines), and the fidelity $F_{\text{av}}^{\text{ign}}$ with ignored ancilla measurement results (dashed lines), as functions of the angle 2θ of intentional X -rotation of the main qubit, $R_1^X(2\theta)$. The simulated protocol of Fig. 4 has duration of 135 ns. We assume the qubits with $T_1 = T_2 = 300$ ns, 500 ns, and 700 ns.

ancilla measurement results 0 and 1 (the probabilities of these results are then $\text{Tr}\rho_{0,j}$ and $\text{Tr}\rho_{1,j}$). The averaged preservation fidelity with ignored measurement results is then (see Appendix) $F_{\text{av}}^{\text{ign}} = (1/6) \sum_j \text{Tr}[(\rho_{0,j} + \rho_{1,j})\rho_j^{\text{in}}]$, where $\rho_j^{\text{in}} = |\psi_j\rangle\langle\psi_j|$ is the unchanged initial state. The averaged (weighted) QED fidelity is then $\tilde{F}_{\text{av}}^{\text{qec}} = \sum_j \text{Tr}(\rho_{0,j}\rho_j^{\text{ideal}}) / \sum_j \text{Tr}\rho_{0,j}$, and the QEC fidelity is $F_{\text{av}}^{\text{qec}} = (1/6) \sum_j \text{Tr}[(\rho_{0,j} + \rho_{1,j}^{\text{corr}})\rho_j^{\text{in}}]$, where the corrected density matrix $\rho_{1,j}^{\text{corr}}$ is obtained from $\rho_{1,j}$ by applying the ideal correcting operations (X, Y, Z, I) discussed in the previous subsection.

Figure 5 shows the average fidelities $\tilde{F}_{\text{av}}^{\text{qec}}$ (solid lines), $F_{\text{av}}^{\text{qec}}$ (dotted lines), and $F_{\text{av}}^{\text{ign}}$ (dashed lines), as functions of the rotation angle 2θ (in units of π) for the intentional X -rotation of the main qubit, $R_1^X(2\theta)$. The three sets of lines are for three values of $T_1 = T_2$: 300 ns, 500 ns, and 700 ns. Note that we present the average fidelities F_{av} , but they can be easily converted into the process matrix fidelities F_χ via Eq. (2). Also note that the range from $1/3$ to 1 for F_{av} (used for the vertical axis in Fig. 5) corresponds to the range from 0 to 1 for F_χ .

From Fig. 5 we see that even for $T_1 = T_2 = 300$ ns the QED fidelity is significantly higher than the fidelity with ignored measurement result (recall that the procedure duration is 135 ns). The difference between $\tilde{F}_{\text{av}}^{\text{qec}}$ and $F_{\text{av}}^{\text{ign}}$ becomes larger for longer decoherence time (500 ns and 700 ns). The QEC fidelity is below the QED fidelity (and even below $F_{\text{av}}^{\text{ign}}$) for small θ , but becomes above $\tilde{F}_{\text{av}}^{\text{qec}}$ and $F_{\text{av}}^{\text{ign}}$ at large θ .

It is interesting to notice that $F_{\text{av}}^{\text{ign}}$ at $2\theta \approx \pi$ is much closer to the ideal value $1/3$ [see Eq. (48)] than to the ideal value 1 at $2\theta \approx 0$. This property can be understood using the equivalent language of the process fidelity $F_\chi = \text{Tr}(\chi^{\text{desired}}\chi)$ – see Eq. (2). Since the desired operation is the absence of evolution, $F_\chi = \chi_{II}$ in the standard

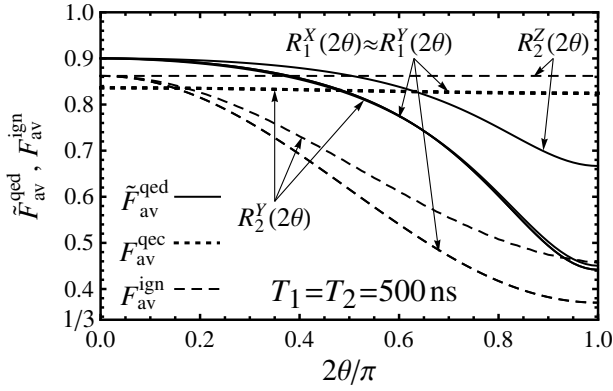


FIG. 6: Same as in Fig. 5, but for four types of intentional qubit state rotations: $R_1^X(2\theta)$, $R_1^Y(2\theta)$, $R_2^Y(2\theta)$, and $R_2^Z(2\theta)$. The qubits with $T_1 = T_2 = 500$ ns are assumed. Results for rotations $R_1^X(2\theta)$ and $R_1^Y(2\theta)$ practically coincide.

notations for the one-qubit 4×4 matrix χ [2, 10, 23, 38]; note that $\chi_{II} + \chi_{XX} + \chi_{YY} + \chi_{ZZ} = 1$. Ideally $\chi_{II} = 1$ for $2\theta = 0$ and $\chi_{XX} = 1$ for $2\theta = \pi$. Since decoherence spreads these ideal unity values to the three other diagonal elements of χ , we would expect that F_χ^{ign} at $2\theta = \pi$ should be (very crudely) three times less than $1 - F_\chi^{\text{ign}}$ at $2\theta = 0$. This roughly corresponds to what we see in Fig. 5.

Figure 5 shows the results only for the X -rotation of the main qubit, $R_1^X(2\theta)$. The results for all four considered rotations, $R_1^X(2\theta)$, $R_1^Y(2\theta)$, $R_2^Y(2\theta)$ and $R_2^Z(2\theta)$, are shown in Fig. 6 for $T_1 = T_2 = 500$ ns. The results for X and Y -rotation of the main qubit are practically indistinguishable from each other. The QED and QEC fidelities for Y -rotation of the ancilla qubit are very close to the corresponding fidelities for the rotation of the main qubit. For Z -rotation of the ancilla qubit the operation with ignored measurement coincides with the QEC operation (because no correction is applied for measurement result 1), and the QED fidelity $\tilde{F}_{\text{av}}^{\text{qcd}}$ is higher than $F_{\text{av}}^{\text{ign}} = F_{\text{av}}^{\text{qec}}$ only at $2\theta \lesssim \pi/2$, and only by a small amount. Obviously, the rotation $R_2^Z(2\theta)$ is not good for demonstrating an advantage of this encoding, in contrast to other rotations.

Overall, from Figs. 5 and 6 we see that the current technology of phase qubits is good enough for demonstrating the operation of the considered two-qubit QED/QEC protocol. In an experiment, the larger value of the QED fidelity in comparison with the case of ignored measurement result is the demonstration that the QED procedure is beneficial. Similarly, the QEC operation can also be demonstrated (though with the caveat discussed in the previous subsection).

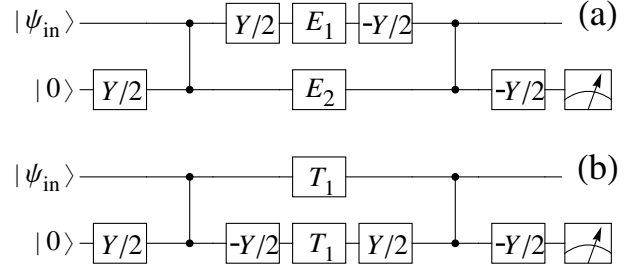


FIG. 7: Modified two-qubit QED/QEC algorithms. The protocol shown in (a) detects/corrects errors due to rotations R_1^Y , R_1^Z , R_2^Y , and R_2^Z ; it can be used to protect from natural pure dephasing of the qubits. The protocol in (b) is designed for error rotations R_1^X , R_1^Y , R_2^X , and R_2^Y . Therefore, it can be used as a QED procedure for errors due to energy relaxation of both qubits (stored in resonators).

C. Related protocols

The protocol of Fig. 4 can be easily modified to change the set of four detectable/correctable error operations. For example, if we desire protection from Y and Z rotations of both qubits [i.e. $R_1^Y(2\theta)$, $R_1^Z(2\theta)$, $R_2^Y(2\theta)$, and $R_2^Z(2\theta)$], we can add $\pm\pi/2$ Y -rotations of the main qubit before and after the error rotations – see Fig. 7(a). Such encoding also protects from natural pure dephasing of both qubits.

For protection from X and Y rotations of both qubits [i.e. $R_1^X(2\theta)$, $R_1^Y(2\theta)$, $R_2^X(2\theta)$, and $R_2^Y(2\theta)$], we can add $\mp\pi/2$ Y -rotations of the ancilla qubit before and after the errors – see Fig. 7(b). Such encoding can be used in the QED mode for the energy relaxation of both qubits. (This procedure essentially realizes the idea of Fig. 1 for two qubits; the only difference is the encoding $\alpha|00\rangle - \beta|11\rangle$ instead of encoding $\alpha|00\rangle + \beta|11\rangle$ considered in Sec. II B.)

In the RezQu architecture based on phase qubits [23, 26], the protocol of Fig. 7(b) can be efficiently used for storing the information in the resonators. We have simulated the operation of this protocol, assuming that the encoding/decoding is done with the phase qubits having relaxation times $T_1 = T_2$, while in between encoding and decoding the information is moved to resonators for a relatively long storage. The procedure (without the storage time) is slightly longer than what was considered in the previous subsection: 155 ns instead of 135 ns (we still do not simulate explicitly the move operations between the qubits and resonators). Solid lines in Fig. 8 show the corresponding QED fidelities $\tilde{F}_{\text{av}}^{\text{qcd}}$ as functions of the single-qubit energy relaxation probability $p = 1 - \exp(-t_{\text{storage}}/T_1^{\text{resonator}})$ during the storage (in experiment [23] $T_1^{\text{resonator}} \gg T_1$, though our results do not need this assumption). The QEC operation is impossible in this case (for real energy relaxation in resonators); however, as seen from Fig. 8, the QED operation can be reliably demonstrated experimentally.

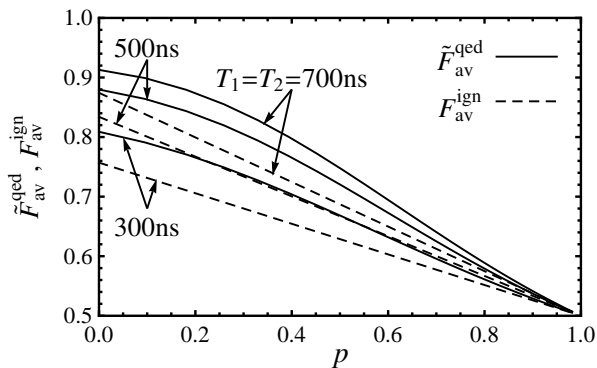


FIG. 8: Average QED fidelity $\tilde{F}_{\text{av}}^{\text{qed}}$ (solid lines) for the two-qubit protocol of Fig. 7(b), as a function of the single-qubit energy relaxation probability $p = 1 - \exp(-t_{\text{storage}}/T_1^{\text{resonator}})$ during information storage in resonators. Dashed lines show average fidelity $F_{\text{av}}^{\text{ign}}$ when the measurement result is ignored. The encoding/decoding is done with phase qubits having significantly shorter relaxation times $T_1 = T_2$ (300 ns, 500 ns, and 700 ns); the assumed duration of the procedure (excluding storage time) is 155 ns.

IV. CONCLUSION

In Sec. II we have analyzed the performance of N -qubit repetitive quantum codes in the presence of energy relaxation. As expected, these codes are not usable for quantum error correction. However, they can be used for quantum error detection. The best QED performance for weak energy relaxation is provided by the 3-qubit repetitive encoding [see Eq. (40) and Fig. 3(a)], while the 2-qubit encoding is sufficient and gives only slightly lower fidelity [see Eq. (32)]. We have found that the main contribution to the QED infidelity for $N \geq 3$ comes from the non-unitary change of the quantum state in the case when no relaxation happens. Therefore, the QED infidelity can be strongly decreased if the QED algorithm is complemented with partial quantum measurement or, alternatively, if the protocol is divided into the even number of cycles and complemented with π -pulses in between (this resembles dynamical decoupling, though only superficially). In this case the fidelity improves with dividing the total duration into a larger number of cycles and using more qubits for the encoding [see Eq. (43)].

Note that the QED fidelity cannot be introduced in the usual way [as $F_\chi = \text{Tr}(\chi_{\text{desired}}\chi)$] via the process χ -matrix. In the analysis we have used the state fidelity, averaged over the Bloch sphere, with the usual conversion into F_χ via Eq. (2). For the state fidelity averaged with the weight proportional to the selection probability (denoted $\tilde{F}_{\text{av}}^{\text{qed}}$) the usual trick of averaging over the 6 initial states can be used (see Appendix), while for the state fidelity averaged with uniform weight (denoted $F_{\text{av}}^{\text{qed}}$) we had to average over the Bloch sphere explicitly, using Eqs. (9)–(17). In the analysis we used unraveling of the decoherence evolution into the “error scenarios”, which

is in general similar to the standard approach used in the quantum error correction, but is different in the way that each scenario describes a non-unitary process.

In Sec. III we have considered simple two-qubit protocols of quantum error detection/correction, suitable for present-day experiments with superconducting phase qubits [23]. In the protocol of Fig. 4 the errors are simulated by intentional unitary rotations of the qubit states (two types of rotations for each qubit). In this case not only the QED, but also the QEC operation is possible if we know the applied type of error rotation. Most importantly, this experiment would demonstrate the QEC “miracle” of converting continuous quantum errors into discrete errors, which are then correctable. The numerical simulations (Figs. 5 and 6) with account of decoherence during the protocol show that the experimental QED and QEC fidelities are expected to be significantly higher than the fidelity with ignored result of the ancilla qubit measurement. Therefore, the QED and QEC benefits can be demonstrated experimentally.

A slightly different protocol, shown in Fig. 7(b), can be used as a QED procedure for errors due to natural energy relaxation of qubits stored in resonators of a RezQu-architecture device [23, 26] based on phase qubits. The numerical simulations (Fig. 8) show that such experiment can also be realized with the present-day technology, demonstrating the benefits of encoding a logical qubit in several (two in this case) physical qubits. While the measurement-free QEC experiment has been recently realized with superconducting transmon qubits [15], the experiments proposed and analyzed in this paper would be the first measurement-based QED/QEC protocols realized with superconducting qubits.

The authors thank John Martinis, Andrew Cleland, and Matteo Mariantoni for fruitful discussions. The work was supported by the IARPA under ARO Grant No. W911NF-10-1-0334.

Appendix A

In this appendix we prove that no additional unitary operation can improve the fidelity of the protocol discussed in Sec. II (for 2-qubit or N -qubit encoding) in the case of “no error” measurement result (0 or $\mathbf{0}$). We also prove that for a measurement result which indicates an error, the optimal correction is either identity or the π -pulse, exchanging $|0\rangle$ and $|1\rangle$. Along the way we also discuss the trick [27, 28] of using only 6 initial states for averaging the state fidelity over the Bloch sphere.

Let us first consider an arbitrary (not necessarily trace-preserving) linear one-qubit quantum operation, which transforms initial states $|1\rangle$, $|0\rangle$, $|\pm\rangle \equiv (|0\rangle \pm |1\rangle)/\sqrt{2}$, $|\pm i\rangle \equiv (|0\rangle \pm i|1\rangle)/\sqrt{2}$ into the density matrices ρ_0 , ρ_1 , ρ_\pm , $\rho_{\pm i}$. The center of the Bloch sphere ($|0\rangle\langle 0| + |1\rangle\langle 1|$)/2 = $I/2$ is transformed into ρ_c . Because of the linearity, only four linearly independent initial states are

sufficient to define the operation. So, for an initial state with the Bloch sphere coordinates $\{x, y, z\}$,

$$\rho_{\text{in}} = (I + xX + yY + zZ)/2, \quad (\text{A1})$$

where $\{X, Y, Z\}$ are the Pauli matrices ($x = 1$ corresponds to $|+\rangle$, $y = 1$ corresponds to $|+i\rangle$, $z = 1$ corresponds to $|0\rangle$), the final state is

$$\rho_{\text{fin}} = \rho_c + x(\rho_+ - \rho_c) + y(\rho_{+i} - \rho_c) + z(\rho_0 - \rho_c). \quad (\text{A2})$$

To compare this operation with a unitary U , we calculate the state fidelity $\text{Tr}(\rho_{\text{fin}}\rho_{\text{fin}}^U)$ (the superscript U in a notation means that it relates to the unitary U),

$$F_{\text{st}} = \text{Tr}\{[\rho_c + x(\rho_+ - \rho_c) + y(\rho_{+i} - \rho_c) + z(\rho_0 - \rho_c)] \times [\rho_c^U + x(\rho_+^U - \rho_c^U) + y(\rho_{+i}^U - \rho_c^U) + z(\rho_0^U - \rho_c^U)]\}. \quad (\text{A3})$$

Note that $\rho_c^U = I/2$, since a unitary operation does not change the Bloch sphere center. In averaging F_{st} over the Bloch sphere we average over the coordinates $\{x, y, z\}$ and use the obvious relations $\bar{x} = \bar{y} = \bar{z} = \bar{xy} = \bar{xz} = \bar{yz} = 0$, $\bar{x^2} = \bar{y^2} = \bar{z^2} = 1/3$, this obtaining

$$\begin{aligned} \bar{F} &= \frac{1}{2}\text{Tr}\rho_c + \frac{1}{3}\text{Tr}[(\rho_+ - \rho_c)(\rho_+^U - \rho_c^U) \\ &\quad + (\rho_{+i} - \rho_c)(\rho_{+i}^U - \rho_c^U) + (\rho_0 - \rho_c)(\rho_0^U - \rho_c^U)]. \quad (\text{A4}) \end{aligned}$$

Note that in general we deal here with non-normalized density matrices, in contrast to the formalism used in Sec. II. Therefore, compared with notations of Sec. II, $\bar{F} = F_{\text{av}} = \tilde{F}_{\text{av}}$ only for a trace-preserving operation, while for a non-trace-preserving operation $\bar{F} = \tilde{F}_{\text{av}}\bar{P}$, where \bar{P} is the average probability of selection [see Eq. (24)], and there is no direct relation between \bar{F} and F_{av} .

Using Eq. (A4) it is easy to see why averaging over the Bloch sphere is equivalent to averaging over only 6 initial states: $|0\rangle$, $|1\rangle$, $|\pm\rangle$, and $|\pm i\rangle$. The state fidelity F_+ for the initial state $|+\rangle$ is given by Eq. (A3) with $x = 1$ and $y = z = 0$. The state fidelity F_- for the initial state $|-\rangle$ is similar, but $x = -1$. It is easy to obtain the sum, $F_+ + F_- = \text{Tr}\rho_c + 2\text{Tr}[(\rho_+ - \rho_c)(\rho_+^U - \rho_c^U)]$, which is similar to the terms in Eq. (A4). Similarly finding the sums $F_{+i} + F_{-i}$ and $F_0 + F_1$, we obtain [27, 28]

$$\bar{F} = (F_0 + F_1 + F_+ + F_- + F_{+i} + F_{-i})/6. \quad (\text{A5})$$

Note that this relation remains valid for non-trace-preserving operations, when we are working with a linear operation and non-normalized states. The same six-point-averaging relation is valid for the average probability of selection \bar{P} , because $P = \text{Tr}\rho_{\text{fin}}$ and therefore $\bar{P} = \text{Tr}\rho_c$ (even two-point averaging is sufficient for \bar{P} , when we choose two opposite points on the Bloch sphere). Therefore the six-point-averaging trick is useful for finding $\tilde{F}_{\text{av}} = \bar{F}/\bar{P}$.

Now let us discuss why an additional unitary cannot improve the QEC protocols of Sec. II when the ‘‘no error’’ measurement result 0 (or $\mathbf{0}$) is obtained. The final state in this case is an incoherent mixture of the results of two linear operations:

$$\alpha|0\rangle + \beta|1\rangle \rightarrow \alpha|0\rangle + k\beta|1\rangle, \quad \alpha|0\rangle + \beta|1\rangle \rightarrow \tilde{k}\beta|0\rangle, \quad (\text{A6})$$

where the real positive constants k and \tilde{k} should obviously satisfy inequality $k^2 + \tilde{k}^2 \leq 1$. For this operation it is easy to find explicitly

$$\rho_c = (1 + \tilde{k}^2 + k^2)I/4 + (1 + \tilde{k}^2 - k^2)Z/4, \quad (\text{A7})$$

$$\rho_+ = \rho_c + kX/2, \quad \rho_{+i} = \rho_c + kY/2, \quad \rho_0 = (Z + I)/2. \quad (\text{A8})$$

Then using Eq. (A4) we obtain

$$\begin{aligned} \bar{F} &= \frac{1}{4}(1 + k^2 + \tilde{k}^2) + \frac{1}{6}\text{Tr}[kX(\rho_+^U - \rho_c^U) \\ &\quad + kY(\rho_{+i}^U - \rho_c^U) + \frac{1 - \tilde{k}^2 + k^2}{2}Z(\rho_0^U - \rho_c^U)]. \quad (\text{A9}) \end{aligned}$$

(Note that comparing the operation with U we assume the correction operation U^\dagger .) Optimizing each term under the trace over the unitary U separately, we see that the first term is maximized by unitaries, which transform $|+\rangle \rightarrow |+\rangle$; the maximum for the second term is achieved when $|+i\rangle \rightarrow |+i\rangle$, and the maximum for the third term is achieved when $|0\rangle \rightarrow |0\rangle$ (note that $k \geq 0$ and $1 - \tilde{k}^2 + k^2 \geq 0$). Since the no-evolution operation satisfies all these conditions, it provides the maximum fidelity,

$$U_{\text{best}} = I, \quad \bar{F} = \frac{1 + k + k^2 + \tilde{k}^2/2}{3}. \quad (\text{A10})$$

Note that the average probability of the process (A6) is $\bar{P} = (1 + k^2 + \tilde{k}^2)/2$, so $\tilde{F}_{\text{av}} = (2/3)(1 + k + k^2 + \tilde{k}^2)/(1 + k^2 + \tilde{k}^2)$. In particular, this is an alternative way of deriving Eq. (34) by using $k = \sqrt{1 - p_1}\sqrt{1 - p_2}$ and $\tilde{k} = \sqrt{p_1 p_2}$.

Now let us discuss what is the optimal unitary correction operation after obtaining the measurement result 1 in 2-qubit encoding or any result except $\mathbf{0}$ in N -qubit encoding. Then the resulting state is an incoherent mixture of two linear operations:

$$\alpha|0\rangle + \beta|1\rangle \rightarrow k\beta|1\rangle, \quad \alpha|0\rangle + \beta|1\rangle \rightarrow \tilde{k}\beta|0\rangle. \quad (\text{A11})$$

Finding explicitly the resulting density matrices

$$\rho_0 = 0, \quad \rho_c = \rho_+ = \rho_{+i} = \frac{\tilde{k}^2}{2}|0\rangle\langle 0| + \frac{k^2}{2}|1\rangle\langle 1|, \quad (\text{A12})$$

we obtain from Eq. (A4)

$$\bar{F} = \frac{k^2 + \tilde{k}^2}{4} + \frac{k^2 - \tilde{k}^2}{12}\text{Tr}[Z(\rho_0^U - \rho_c^U)]. \quad (\text{A13})$$

Therefore if $k \geq \tilde{k}$, then the maximum fidelity $\bar{F}_{\text{max}} = (2k^2 + \tilde{k}^2)/6$ is achieved for any unitary U , which does not change $|0\rangle$ (same for the correcting operation U^\dagger). However, if $k \leq \tilde{k}$, then the optimal U transforms $|0\rangle \rightarrow |1\rangle$ (same for U^\dagger) and $\bar{F}_{\text{max}} = (k^2 + 2\tilde{k}^2)/6$.

-
- [1] P. W. Shor, Phys. Rev. A **52**, R2493 (1995); A. M. Steane, Phys. Rev. Lett. **77**, 793 (1996); A. R. Calderbank and P. W. Shor, Phys. Rev. A **54**, 1098 (1996); D. Gottesman, Phys. Rev. A **54**, 1862 (1996).
- [2] M. A. Nielsen and I. L. Chuang, *Quantum computation and quantum information* (Cambridge University Press, Cambridge, 2000).
- [3] J. Preskill, Proc. R. Soc. A **454**, 385 (1998).
- [4] S. B. Bravyi and A. Y. Kitaev, quant-ph/9811052; E. Dennis, A. Kitaev, A. Landahl, and J. Preskill, J. Math. Phys. **43**, 4452 (2002); A. G. Fowler, A. M. Stephens, and P. Groszkowski, Phys. Rev. A **80**, 052312 (2009).
- [5] D. G. Cory, M. D. Price, W. Maas, E. Knill, R. Laflamme, W. H. Zurek, T. F. Havel, and S. S. Somaroo, Phys. Rev. Lett. **81**, 2152 (1998).
- [6] E. Knill, R. Laflamme, R. Martinez, and C. Negrevergne, Phys. Rev. Lett. **86**, 5811 (2001).
- [7] N. Boulant, L. Viola, E. M. Fortunato, and D. G. Cory, Phys. Rev. Lett. **94**, 130501 (2005).
- [8] O. Moussa, J. Baugh, C. A. Ryan, and R. Laflamme, Phys. Rev. Lett. **107**, 160501 (2011).
- [9] J. Chiaverini, D. Leibfried, T. Schaetz, M. D. Barrett, R. B. Blakestad, J. Britton, W. M. Itano, J. D. Jost, E. Knill, C. Langer, R. Ozeri, and D. J. Wineland, Nature **432**, 602 (2004).
- [10] P. Schindler, J. T. Barreiro, T. Monz, V. Nebendahl, D. Nigg, M. Chwalla, M. Hennrich, and R. Blatt, Science **332**, 1059 (2011).
- [11] T. B. Pittman, B. C. Jacobs, and J. D. Franson, Phys. Rev. A **71**, 052332 (2005).
- [12] T. Aoki, G. Takahashi, T. Kajiya, J. Yoshikawa, S. L. Braunstein, P. van Loock, and A. Furusawa, Nature Phys. **5**, 541 (2009).
- [13] M. Lassen, M. Sabuncu, A. Huck, J. Niset, G. Leuchs, N. J. Cerf, and U. L. Andersen, Nature Photonics **4**, 700 (2010).
- [14] X. C. Yao, T. X. Wang, H. Z. Chen, W. B. Gao, A. G. Fowler, R. Raussendorf, Z. B. Chen, N. L. Liu, C. Y. Lu, Y. J. Deng, Y. A. Chen, and J. W. Pan, Nature **482**, 489 (2012).
- [15] M. D. Reed, L. DiCarlo, S. E. Nigg, L. Sun, L. Frunzio, S. M. Girvin, and R. J. Schoelkopf, Nature **482**, 382 (2012).
- [16] N. C. Menicucci and C. M. Caves, Phys. Rev. Lett. **88**, 167901 (2002).
- [17] John Clarke and F. K. Wilhelm, Nature **453**, 1031 (2008); B. G. Levi, Phys. Today **62**, no. 7, 14 (2009); I. Siddiqi, Supercond. Sci. Technol. **24**, 091002 (2011); S. M. Girvin, M. H. Devoret, and R. J. Schoelkopf, Phys. Scr. **T137**, 014012 (2009).
- [18] Quant. Inf. Proc. **8**, no. 2 (2009): Special issue on quantum computing with superconducting qubits.
- [19] J. M. Martinis, Quant. Inf. Proc. **8**, 81 (2009).
- [20] K. Keane and A. N. Korotkov, Bull. Am. Phys. Soc. 2011.MAR.D29.14.
- [21] L. Tornberg, M. Wallquist, G. Johansson, V. S. Shumeiko, and G. Wendin, Phys. Rev. B **77**, 214528 (2008).
- [22] B. R. Johnson, M. D. Reed, A. A. Houck, D. I. Schuster, L. S. Bishop, E. Ginossar, J. M. Gambetta, L. DiCarlo, L. Frunzio, S. M. Girvin, and R. J. Schoelkopf, Nature Phys. **6**, 663 (2010).
- [23] M. Mariantoni, H. Wang, T. Yamamoto, M. Neeley, R. C. Bialczak, Y. Chen, M. Lenander, E. Lucero, A. D. O'Connell, D. Sank, M. Weides, J. Wenner, Y. Yin, J. Zhao, A. N. Korotkov, A. N. Cleland, and J. M. Martinis, Science **334**, 61 (2011).
- [24] R. Laflamme, C. Miquel, J. P. Paz, W. H. Zurek, Phys. Rev. Lett. **77**, 198 (1996); C. H. Bennett, D. P. DiVincenzo, J. A. Smolin, and W. K. Wootters, Phys. Rev. A **54**, 3824 (1996).
- [25] D. Leung, L. Vandersypen, X. Zhou, M. Sherwood, C. Yannoni, M. Kubinec, and I. Chuang, Phys. Rev. A **60**, 1924 (1999).
- [26] A. Galiutdinov, A. N. Korotkov, and J. M. Martinis, Phys. Rev. A **85**, 042321 (2012).
- [27] M. A. Nielsen, Phys. Lett. A **303**, 249 (2002); M. Horodecki, P. Horodecki, and R. Horodecki, Phys. Rev. A **60**, 1888 (1999).
- [28] M. D. Bowdrey, D. K. L. Oi, A. J. Short, K. Banaszek, and J. A. Jones, Phys. Lett. A **294**, 258 (2002).
- [29] A. N. Korotkov and K. Keane, Phys. Rev. A **81**, 040103(R) (2010).
- [30] N. Katz, M. Ansmann, R. C. Bialczak, E. Lucero, R. McDermott, M. Neeley, M. Steffen, E. M. Weig, A. N. Cleland, J. M. Martinis, and A. N. Korotkov, Science **312**, 1498 (2006).
- [31] M. Al-Amri, M. O. Scully, and M. S. Zubairy, J. Phys. B **44**, 165509 (2011); Q. Sun, M. Al-Amri, L. Davidovich, and M. S. Zubairy, Phys. Rev. A **82**, 052323 (2010).
- [32] Y.-S. Kim, J.-C. Lee, O. Kwon, and Y.-H. Kim, Nature Phys. **8**, 117 (2012); J.-C. Lee, Y.-C. Jeong, Y.-S. Kim, and Y.-H. Kim, Opt. Express **19**, 16309 (2011).
- [33] D. W. Leung, M. A. Nielsen, I. L. Chuang, and Y. Yamamoto, Phys. Rev. A **56**, 2567 (1997).
- [34] A. S. Fletcher, P. W. Shor, and M. Z. Win, IEEE Trans. Inf. Theory **54**, 5705 (2008); P. W. Shor, G. Smith, J. A. Smolin, and B. Zeng, IEEE Trans. Inf. Theory **57**, 7180 (2011).
- [35] A. N. Korotkov and A. N. Jordan, Phys. Rev. Lett. **97**, 166805 (2006); N. Katz, M. Neeley, M. Ansmann, R. C. Bialczak, M. Hofheinz, E. Lucero, A. O'Connell, H. Wang, A. N. Cleland, J. M. Martinis, and A. N. Korotkov, Phys. Rev. Lett. **101**, 200401 (2008).
- [36] L. Viola, E. Knill, and S. Lloyd, Phys. Rev. Lett. **82**, 2417 (1999).
- [37] L. P. Pryadko and G. Quiroz, Phys. Rev. A **80**, 042317 (2009).
- [38] T. Yamamoto, M. Neeley, E. Lucero, R. C. Bialczak, J. Kelly, M. Lenander, M. Mariantoni, A. D. O'Connell, D. Sank, H. Wang, M. Weides, J. Wenner, Y. Yin, A. N. Cleland, and J. M. Martinis, Phys. Rev. B **82**, 184515 (2010).